

Figure 1 Paleogeographical map showing locations of the study sections at Meishan (1) and the P/Tr boundary sections (Erwin 1993, 1994; Wang *et al.* 1994; Wignall & Twitchett 1996; Retallack *et al.* 1998; Wignall *et al.* 1998) discussed in this paper. The base map follows Ziegler *et al.* (1998). Locality 2 is the primary depositional site of the P/Tr boundary in Japan (Isozaki 1997).

South Africa, Madagascar, India and Antarctica); and (ii) non-marine low-latitude regions (5% in South China) (Figure 1; Table 1). Riccardi *et al.* (2007) also considered that the decreasing extent and intensity of $\delta^{13}\text{C}$ ($\frac{1}{4}\delta^{13}\text{C}_{\text{carb}} - \delta^{13}\text{C}_{\text{org}}$) averaged a negative shift of * 5%, although they may vary among locations across the entire Paleo-Tethys.

Accordingly, apart from the dramatic biotic extinction itself, the pronounced global negative shift of $\delta^{13}\text{C}$ also characterises the P/Tr transition worldwide and has been regarded as an important marker of the end-Permian extinction event (Baud *et al.* 1989). However, the relationship between negative shift of $\delta^{13}\text{C}$ and biotic mass extinction has long remained in dispute (Twitchett *et al.* 2001; Payne *et al.* 2004). This is probably, at least in part, because the end-Permian mass extinction horizon has not been precisely calibrated in most of the P/Tr boundary sections around the world.

In Meishan, the end-Permian mass extinction has been confirmed to be abrupt, monogenic and the event horizon has been calibrated to the base of Bed 25 (Jin *et al.* 2000; Kaiho *et al.* 2001; Erwin *et al.* 2002). Kaiho *et al.* (2006a) further precisely calibrated the event horizon to the Layer 24e-2, an interval between 3.1 cm and 1.9 cm below the top of Bed 24e, based on detailed paleontological, sedimentological and isotopic geochemical studies of the event horizons at the same section. More recently, Xie *et al.* (2005, 2007a) and Yin *et al.* (2007a, b) clarified that the end-Permian mass extinction could be episodic rather than abrupt and monogenic based on their biogeochemical (biomarker analysis) and paleoecological studies from Meishan. The event horizons can be calibrated to the bases of Bed 24e, Bed 25

and Bed 28, respectively at Meishan (Xie *et al.* 2005; Yin *et al.* 2007a, b). These authors also agreed that the event recorded in the base of Bed 25 was the main episode of the P/Tr crisis. Here, we also measured stable carbon isotope ratio ($\delta^{13}\text{C}$) of carbonate (bulk and brachiopod shell) and all organic matter, marine/terrestrial kerogen percentage, and total organic carbon percentage based on our samples from the P/Tr boundary beds at Meishan. The integration of various geochemical signals enables us to enhance our understanding of anomalous carbon isotopic excursions and the associated biotic extinction events recorded in Meishan. As a consequence, this study aims specifically to evaluate: (i) the relationship between the negative shift of $\delta^{13}\text{C}$, D^{13}C and the end-Permian mass extinction; (ii) the negative shift process of $\delta^{13}\text{C}$; and (iii) the potential causes. Previously published $\delta^{13}\text{C}$ data from various quarries of the Meishan section are discussed in terms of possible diagenetic and weathering effects.

STUDY SECTION AND CHRONOSTRATIGRAPHY

The Meishan section is located at the northern Meishan township, about 190 km west of Shanghai city in eastern China (Figure 1). The Meishan area was situated at the low-latitude, tropical region of the eastern Paleo-Tethys during the P/Tr transition (Ziegler *et al.* 1998). The Meishan section comprises seven well-exposed quarries labelled by Sheng *et al.* (1984) as Meishan sections A–E and Z (see also Yin *et al.* 2001; Chen *et al.* 2002, 2005). Of these, the Meishan section D was selected as the Global

Table 1 Negative shift of stable carbon isotope ratio at the end-Permian mass extinction horizons around the world.

Sampling areas	Decrease in $\delta^{13}\text{C}$ (%)	Carbonate/organic carbon	Reference
Marine			
Kuh-e-Ali Bashi, Iran	3.0	Carbonate	Baud <i>et al.</i> (1989)
Vedi, Armenia	1.5	Carbonate	Baud <i>et al.</i> (1989)
Sovelashen, Armenia	2.6	Carbonate	Baud <i>et al.</i> (1989)
Emarat, Iran	3.1	Carbonate	Baud <i>et al.</i> (1989)
Idrijca, Slovenia	1.8	Carbonate	Baud <i>et al.</i> (1989)
Idrijca, Slovenia	2.1	Carbonate	Dolenec <i>et al.</i> (2001)
CurukDag, Turkey	2.5	Carbonate	Baud <i>et al.</i> (1989)
Kemer, Turkey	2.8	Carbonate	Baud <i>et al.</i> (1989)
Nammal, Pakistan	3.0	Carbonate	Baud <i>et al.</i> (1989)
Thongde, India	2.4	Carbonate	Baud <i>et al.</i> (1989)
Shangsi, Sichuan, China	4.3	Carbonate	Baud <i>et al.</i> (1989)
Shangsi, Sichuan, China	4.4	Carbonate	Li <i>et al.</i> (1986)
Shangsi, Sichuan, China	4.0	Carbonate	Riccardi <i>et al.</i> (2007)
Meishan, Zhejiang, China	8.0	Carbonate	Xu <i>et al.</i> (1989); Xu & Yan (1993)
Meishan, Zhejiang, China	3.5	Carbonate	Xu <i>et al.</i> (1989)
Meishan, Zhejiang, China	4.3	Carbonate	Baud <i>et al.</i> (1989)
Meishan, Zhejiang, China	3.0	Carbonate	Jin <i>et al.</i> (2000)
Meishan, Zhejiang, China	3.0	Carbonate	Cao <i>et al.</i> (2002)
Meishan, Zhejiang, China	4.0	Organic carbon	Cao <i>et al.</i> (2002)
Meishan, Zhejiang, China	4.0	Carbonate	Grice <i>et al.</i> (2005)
Meishan, Zhejiang, China	3.0	Carbonate	Kaiho <i>et al.</i> (2006a)
Meishan, Zhejiang, China	4.0	Carbonate	Riccardi <i>et al.</i> (2007)
Meishan, Zhejiang, China	5.0	Carbonate	Xie <i>et al.</i> (2007b)
Meishan, Zhejiang, China	3.0	Carbonate	This study
Meishan, Zhejiang, China	3.0	Organic carbon	This study
Taiping, Guizhou, China	3.0	Carbonate	Krull <i>et al.</i> (2004)
Taiping, Guizhou, China	3.0	Organic carbon	Krull <i>et al.</i> (2004)
Heping, Guizhou, China	6.0	Carbonate	Krull <i>et al.</i> (2004)
Heping, Guizhou, China	3.0	Organic carbon	Krull <i>et al.</i> (2004)
Tesero, north Italy	2.5	Carbonate	Magaritz <i>et al.</i> (1988)
Kamura, Japan	2.0	Carbonate	Musashi <i>et al.</i> (2001)
Kamura, Japan	2.0	Organic carbon	Musashi <i>et al.</i> (2001)
Taho, Japan	1.3	Carbonate	Musashi <i>et al.</i> (2001)
Taho, Japan	2.5	Organic carbon	Musashi <i>et al.</i> (2001)
Hambast, Abadeh, Iran	4.0	Carbonate	Heydari <i>et al.</i> (2001)
Hambast, Abadeh, Iran	3.0	Organic carbon	Heydari <i>et al.</i> (2001)
Abadeh, Iran	4.0	Carbonate	Heydari <i>et al.</i> (2001)
Shah Reza, Iran	4.0	Carbonate	Heydari <i>et al.</i> (2001)
Spitsbergen, Norway	5.4	Organic carbon	Wignall <i>et al.</i> (1998)
Gartourkofel, Austria	3.2	Carbonate	Holser <i>et al.</i> (1989)
Spiti Valley, Himalaya	4.0	Organic carbon	Ghosh <i>et al.</i> (2002)
Spiti Valley, Himalaya	2.5	Carbonate	Ghosh <i>et al.</i> (2002)
Williston Lake, Canada	3.5	Organic carbon	Wang <i>et al.</i> (1994)
Non-marine			
Bonaparte Basin, Australia	10.5	Organic carbon	Morante <i>et al.</i> (1994)
Canning Basin, Australia	8.0	Organic carbon	Morante <i>et al.</i> (1994)
Bowen Basin, Australia	6.5	Organic carbon	Morante <i>et al.</i> (1994)
Sydney Basin, Australia	5.0	Organic carbon	Morante (1996)
Bonaparte Basin, Australia	8.0	Organic carbon	Morante (1996)
Wairoa River, New Zealand	16.0	Organic carbon	Krull <i>et al.</i> (2000)
Graphite Peak, Antarctica	20.0	Organic carbon	Krull & Retallack (2000)
Raniganj Coal Field, India	5.0	Organic carbon	Wit <i>et al.</i> (2002)
Wardha and Korar Coalfield, India	3.0	Organic carbon	Wit <i>et al.</i> (2002)
Godavari Coalfield, India	10.0	Organic carbon	Wit <i>et al.</i> (2002)
Talcher Coalfield, India	7.0	Organic carbon	Wit <i>et al.</i> (2002)
Morondava, Madagascar	4.0	Organic carbon	Wit <i>et al.</i> (2002)
Raniganj Coalfield, India	6.0?	Organic carbon	Sarkar <i>et al.</i> (2003)
Chahe, Guizhou, China	5.0	Organic carbon	Peng <i>et al.</i> (2005)

Stratotype for Section and Point (GSSP) of the P/Tr boundary (Yin *et al.* 2001). However, the rocks of the P/Tr boundary beds in this quarry have been strongly

weathered (Bowring *et al.* 1998). In contrast, the P/Tr rocks from the Meishan section A are fairly fresh (Bowring *et al.* 1998; Kaiho *et al.* 2001). At Meishan

section A, the P/Tr succession was deposited in the carbonate ramp setting (Zhang *et al.* 1996) and comprises the Changhsing Formation below and the Yinkeng Formation above.

The uppermost Changhsing Formation (Bed 24e, 20 cm thick), except for the top 3 cm thick strata (layers 24e-2 and 24e-3), comprises dark-grey packstone–wackestone containing abundant calcareous microfossils (Kaiho *et al.* 2006a). Layers 24e-2 and 24e-3 and the overlying Fe–Ni-rich, greyish-black, thin layer (Layer 25-1, 0.1 mm thick) of Bed 25 at the basal Yinkeng Formation are characterised by: (i) low contents of phosphorous and calcium, proxies for biomass; (ii) Ni enrichment; (iii) low values in $^{87}\text{Sr}/^{86}\text{Sr}$ of siliciclastics; and (iv) greyish-black fragments (0.2–10 mm; see also Kaiho *et al.* 2001, 2006a). This 3.01 cm-thick stratum (Layers 24e-2, 24e-3 and 25-1) was therefore interpreted to contain sediments sourced from mantle-induced plume volcanism, which may have triggered the end-Permian mass extinction (Renne *et al.* 1995; Kamo *et al.* 2003; Lamarque *et al.* 2007). The overlying dark, yellowish-orange thin layer (Layer 25-2, 0.3–1 mm thick) consists mostly of gypsum, which yields a $\delta^{34}\text{S}$ value of -15.8% (Kaiho *et al.* 2006a) and thus was not precipitated from seawater. The remaining part of Bed 25 (Layer 25-3, 2–4 cm thick) is light-bluish-grey illite–montmorillonite claystone (white clay) (Yin *et al.* 1992; Chai *et al.* 1992). The overlying black shale interbedded with yellow thin claystone (Bed 26, 6–8 cm thick) is overlain by a marl (Bed 27). The P/Tr boundary is placed at the middle of Bed 27 (Yin *et al.* 2001). Fresh-rock samples have been collected continuously from the strata spanning the 60 cm-thick interval (Bed 24e to Bed 29), which contains both the extinction horizon (Jin *et al.* 2000) and P/Tr boundary at the Meishan section A.

Minimum values in carbonate, organic carbon, and kaolinite (Kaiho *et al.* 2001) in the white clay (Layer 25-3) suggest rapid sedimentation and support the view that the white clay originated from volcanic ash (Chai *et al.* 1992; Yin *et al.* 1992). The volcanic origin indicates that the white clay could have been deposited within very short time (51 ka).

Radiometric ages of Beds 25 and 28 dated by various laboratories are slightly different [respectively: 251.4 ± 0.3 Ma and 250.7 ± 0.3 Ma (Bowring *et al.* 1998); 252.6 ± 0.2 Ma and 252.5 ± 0.3 Ma (Mundil *et al.* 2001, 2004); 252.25 ± 0.06 Ma and 252.10 ± 0.07 Ma, Bowring *et al.* (2007)].

METHODS

Sampling

The complete rock-log spanning a 60 cm-thick interval (Beds 24e to 29) was collected from Meishan sections A and D. Samples of large blocks were taken by utilising both rock saw and large hammer to guarantee completeness of samples from the event horizons, and then hard sedimentary rocks (limestone and marlstone) were cut in 1 or 2 cm intervals in the laboratory.

Carbon isotopes

The carbon isotope ratio of bulk carbonate sediments ($\delta^{13}\text{C}_{\text{carb}}$) and samples of brachiopod shell were measured using a Finnigan Mat Delta-S mass spectrometer at Tohoku University. All isotopic values are reported relative to VPDB standard. The overall uncertainties of $\delta^{13}\text{C}$ are $+0.1\%$.

The isotopic composition of total organic carbon ($\delta^{13}\text{C}_{\text{org}}$) was measured at Shoko Co. Ltd, Tokyo. Powdered samples were treated with 6N HCl to remove carbonate and then were measured using an elemental analyser combined with a Finnigan delta Plus Advantage mass spectrometer in online mode. Standard deviation of the $\delta^{13}\text{C}$ measurement was generally 50.2% .

Kerogen

Whole-rock samples were crushed into a fine powder in an agate mortar. Powdered rock samples (5–10 g) were treated sequentially within a water-bath shaker as follows: HCl 6M (100 mL, 60°C, 12 h), HCl 12M/HF 46% (1/1 v/v) (100 mL, 60°C, 24 h), HCl 6M (100 mL, 60°C, 4 h). After each treatment, the supernatant liquid was removed after centrifuging (3000 rpm, 10 min). The kerogen residue was sequentially washed with HCl 6M (6/2) and distilled water (6/5), recovered, and freeze-dried under vacuum.

Wet residual particles obtained after HCl/HF treatment were siphoned and dropped onto slides, and were mounted in permanent slides for microscopic examination. A total of 300 particles of kerogen macerals were point-counted per slide under a transmitted-light microscope. Fluorescence-light microscope observation was employed to differentiate the marine-origin amorphous kerogens from terrestrially derived ones since the former tend to fluoresce significantly (Sawada & Akiyama 1994). However, this method should be applied with caution because the terrigenous amorphous kerogen, formed by the high degradation of herbaceous macerals such as sporinite and cutinite, might fluoresce (Smith 1984; Oboh-Ikuenobe *et al.* 1997) and mature amorphous kerogen does not fluoresce even if it was derived from marine organisms (K. Sawada unpubl. data). Consequently, we identified amorphous kerogens based on both the fluorescence and morphology under transmitted-light microscopy (Boussafir *et al.* 1995). The insoluble organic matter (kerogens) from the Meishan section A includes six types. Of these, fluorescent amorphous kerogen (FAK), brown amorphous kerogen (brown AK) and orange amorphous kerogen (orange AK) are marine kerogen. Non-fluorescent amorphous kerogen (NFAK), woody kerogen and herbaceous kerogen are terrestrial kerogen. From the point count data we obtained marine/terrestrial kerogen percentages.

Time-scale

At Meishan, Jin *et al.* (2000 p. 433) estimated the sedimentation rates are 0.03 cm/ka for Beds 25–28, 0.4 cm/ka for Bed 24 and underlying strata, and 1.3 cm/ka for

Bed 29 and overlying strata based on the radiometric data of Bowring *et al.* (1998). The recent radiometric ages of Mundil *et al.* (2001, 2004) indicate that Beds 25–28 represent a duration of 100 ka, which means a depositional rate of 0.22 cm/ka for Beds 26–27 (Beds 25 and 28 are volcanic ashes and were accumulated within very short periods). If both the depositional rates calculated based on radiometric ages of Mundil *et al.* (2001, 2004) for Beds 26–27 and these by Jin *et al.* (2000) for Bed 24 are followed, the sedimentation durations of stratal intervals between horizons 7 10, 0, 10, 18, and 26 cm in height (where 0 cm is the base of Bed 25) are 7 25, 0, 27, 64 and 100 ka, respectively (Figure 2).

RESULTS AND DISCUSSION

Relationship between $\delta^{13}\text{C}$, marine kerogen percentage and total organic carbon

The variations among several geochemical signals [$\delta^{13}\text{C}_{\text{carb}}$, $\delta^{13}\text{C}_{\text{org}}$, D^{13}C , marine kerogen %, $^{87}\text{Sr}/^{86}\text{Sr}$ of siliciclastics and total organic carbon (TOC)] recorded in the P/Tr transition of Meishan (Figure 2) collectively show six geochemical variation zones (GVZ). Of these, GVZ 1 corresponds to the lower-middle parts of Bed 24e-1, GVZ 2 to the upper part of Bed 24e-1,

GVZ 3 to Beds 24e-2, 24e-3, 25-1 and 25-2, GVZ 4 to Bed 25-3, GVZ 5 to Bed 26, and GVZ 6 to Beds 27–29 (Figure 2). Their characterisation is summarised below.

The $\delta^{13}\text{C}$ of marine bulk carbonate underwent a 1% positive shift from 1‰ at 7 13 cm to 2‰ at 7 7 cm in Bed 24e-1 (within GVZ 1), followed by a 1% negative shift from 2‰ at 7 7 cm in Bed 24e-1 to 0‰ in Bed 24e-3 throughout GVZ 2–3. If the above estimate of sedimentation rate for Bed 24e is followed, this negative shift probably took place within * 18 ka. Kaiho *et al.* (2006a) calibrated the P/Tr mass extinction (equating the main episode of the P/Tr event of Yin *et al.* 2007a) to a 12 mm-thick interval with its top 19 mm below the top of Bed 24e at Meishan. If so, the end-Permian mass extinction took place during the latest * 5 ka within this 18 ka period.

It is worth noting that the clay bed (Bed 25 in GVZ 4) has very poor record of $\delta^{13}\text{C}$. Another 1% negative shift is recorded in Bed 26 from 0‰ in the lower part of Bed 26 to 7 1‰ at the middle part of the same bed. We estimate that this stratal interval represents * 13 ka (Figure 2). This $\delta^{13}\text{C}_{\text{carb}}$ excursion is also reinforced by the $\delta^{13}\text{C}$ values measured from brachiopod shells, and the latter indicate the lowest value occurs in mid-Bed 26 (Figure 2). Values of $\delta^{13}\text{C}_{\text{carb}}$ increase by almost 2‰ from mid-Bed 26 to basal Bed 27, and then remain unchanged throughout the upper part of Bed 27 to Bed 29,

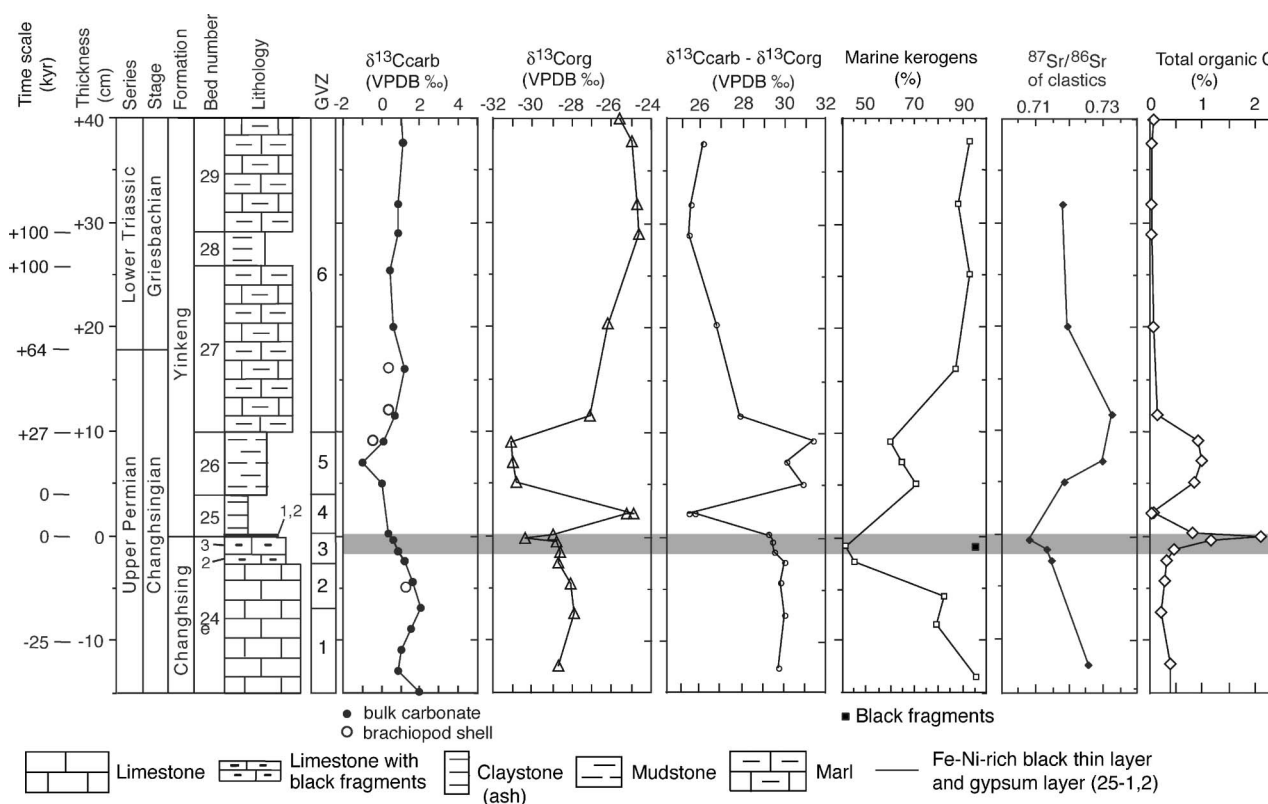


Figure 2 Various geochemical signals ($\delta^{13}\text{C}$ of bulk carbonate, brachiopod shell, and organic matter, marine kerogen %, D^{13}C , $^{87}\text{Sr}/^{86}\text{Sr}$ of clastics and TOC) from the stratal interval between 7 15 cm and 140 cm (relative to the extinction horizon designated as 0 cm) of the P/Tr boundary beds at the Meishan section. Value of $^{87}\text{Sr}/^{86}\text{Sr}$ of clastics follows Kaiho *et al.* (2001). Samples were taken continuously. Datum points were marked in the middle part of each sample interval. A grey band indicates the mass extinction horizon (after Kaiho *et al.* 2006a). Six geochemical variation zones (GVZ 1–6) are recognised from the P/Tr transition. The value of $\delta^{13}\text{C}_{\text{carb}}$ in Bed 25-2 is applied to calculate the value of D^{13}C in Bed 25-3.

suggesting that recovery of the ocean-atmosphere $d^{13}C$ values occurred about 10 cm above the event horizon (or within * 27 ka after the end-Permian event). The entire excursion in $d^{13}C$ lasted * 30 ka from Bed 24e-1 to Bed 26.

Organic $d^{13}C$ also experienced an increase of 1% from 7.29‰ at 7.13 cm to 7.28‰ at 7.7 cm in Bed 24e-1 followed by two-step decreases of 1% from 7.28‰ at 7.4 cm to 7.29‰ at 7.3 cm in Bed 24e-1 and from 7.29‰ at 7.3 to 7.2 cm in Layer 24e-2 to 7.30‰ at 7.1 to 0 cm in Layer 24e-3. This negative shift is followed by a 5% positive shift from 7.30‰ at Layer 24e-3 to 7.25‰ in Layer 25-3, and then $d^{13}C_{org}$ returns to 7.31‰ at the lower part of Bed 26. Then, organic $d^{13}C$ underwent a gradual increase in Bed 27 and remained relatively stable over Beds 28–29 (7.25‰). Except for the high values at Bed 25, organic $d^{13}C$ excursions are comparable with those of bulk carbonate (Figure 2), both indicating a 1% decrease at the extinction horizon in the uppermost Bed 24 (24e-2 and 24e-3) and at Bed 26, respectively. The high values in $d^{13}C_{org}$ at Bed 25 are probably due to high ratios in bacteria/eukaryotes and/or marine kerogen; while the high values in $d^{13}C_{org}$ in Bed 29 are because of high marine kerogen % (* 90%: Figure 2). The marine kerogen percentage curve also shows two lows, occurring at Layers 24e-2, 24e-3 (40–50%) and Bed 26 (60–70%), respectively, reflecting two negative shifts in $d^{13}C_{org}$. This means that the negative shifts in $d^{13}C_{org}$ were due to an increase in terrestrial kerogen (* 7.28‰ VPDB) because the latter has lower $d^{13}C$ values than marine kerogen (* 7.25‰ VPDB) (Figure 2).

The difference between $d^{13}C_{carb}$ and $d^{13}C_{org}$ [i.e. $D^{13}C$ ($4d^{13}C_{carb} - d^{13}C_{org}$)] from GVZ 1 to GVZ 2 in Bed 24e-1 remains unchanged, averaging * 30‰, then shows a marginal change to * 29‰ in GVZ 3 of Bed 24e-2 and 24e-3. $D^{13}C$ decreases dramatically down to * 25‰ in Bed 25-3 (GVZ 4), then increases to * 30–32‰ in Bed 26 (GVZ 5). $D^{13}C$ drops again to * 28‰ in the basal Bed 27 and then gently decreases throughout Beds 27–29 (GVZ 6), eventually dropping to * 26‰ in Bed 29. The decrease in $D^{13}C$ from P/Tr boundary sections is believed to represent a shift from algae/cyanobacteria to less-fractionating phototrophic sulfur bacteria in oceans (Riccardi *et al.* 2007) because the fractionation between CO_2 and organic carbon for the green sulfur bacteria was 7.12.5% (van Breugel *et al.* 2005). Consequently, the dramatic decrease in $D^{13}C$ in Bed 25 indicates an abrupt proliferation of the phototrophic sulfur bacteria immediately after the main episode of the end-Permian mass extinction. Low $D^{13}C$ values throughout Beds 27–29 imply that phototrophic sulfur bacteria may have thrived (* 30% of total biomass) after the main extinction. The abrupt increase in $D^{13}C$ in Bed 26 is here interpreted to be probably due to massive input of terrestrial organic matter (GVZ 5) (Wang 2007; Wang & Visscher 2007), as indicated by the negative shift of $d^{13}C$ discussed above. This result is reinforced by similar study undertaken by Riccardi *et al.* (2006, 2007) at the same section and the interpretation is also consistent with the independent evidence from biomarker analysis (Grice *et al.* 2005; Xie *et al.* 2005).

In summary, a 3% negative shift of $d^{13}C$ in both carbonate and organic matter, occurring within a period of * 30 ka, is recorded from mid-Bed 24e-1 to

mid-Bed 26 at the Meishan section (GVZ 2–5). The decrease in $d^{13}C$ of marine carbonate and all organic matter implies a rapid release of isotopically light carbon to the atmosphere-ocean system during * 30 ka. The middle part of the negative shift corresponds to the end-Permian mass extinction event spanning * 5 ka (Layer 24e-2), and is marked by maxima of total organic carbon (TOC) (2%: Figure 2), Ni (90 and 120 ppm: Kaiho *et al.* 2001, 2006a), a minimum of $^{87}Sr/^{86}Sr$ of siliciclastics and a negative shift of $d^{34}S_{sulfate}$ (GVZ 3) (Kaiho *et al.* 2001, 2006a).

Possible biases of the $d^{13}C$ values from Meishan

Jin *et al.* (2000) reported an exceptionally rapid negative shift in $d^{13}C_{carb}$ within Bed 25 at Meishan (from 2‰ to 7.1‰). However, this rather low value of $d^{13}C_{carb}$ measured from Bed 25 is questionable because, as noted above, the white clay originated from volcanic ash and contains little carbonate. As consequence, it is not possible to measure $d^{13}C_{carb}$ from Bed 25. If the negative shift in $d^{13}C_{carb}$ occurred in an ocean-atmosphere-biosphere system, $d^{13}C_{org}$ in Bed 25 should be much lower than those measured in this study. As a result, the value of $d^{13}C_{carb}$ from Bed 25 is probably due to a diagenetic effect. Recently, Xie *et al.* (2007b) showed that $d^{13}C_{carb}$ values in Bed 25 were similar to those in Bed 26 (7.05 to 0‰).

In addition, Xu & Yan (1993) reported an 8% negative shift of $d^{13}C_{carb}$ from Beds 26 to 27 from the Meishan section D. This result has been accepted by later authors (Bowring *et al.* 1998; Berner 2002). We also obtained rather low values of $d^{13}C_{carb}$ from the Meishan section D. However, when compared with the $d^{13}C_{carb}$ values measured from the same horizons of Meishan section A, the isotopic values obtained from Meishan section D are much lower, and we found that the samples from section D have been much more strongly weathered than those collected from section A. As such, the $d^{13}C_{carb}$ values measured from Meishan section D are unreliable simply due to weathering.

Relation between negative shifts of $d^{13}C$ and biotic mass extinction

As tabulated here (Table 1) and discussed by Corsetti *et al.* (2005), a 2–4% negative shift of $d^{13}C$ has been reported from other marine P/Tr boundary sections around the world. It is comparable with the decreasing values (3%) of $d^{13}C$ recorded in the P/Tr boundary beds at the Meishan section, indicating that this negative shift of $d^{13}C$ is contemporaneous and global. Several studies have explained that the negative shift was due to a decrease in biomass, indicated by a low $d^{13}C$ value (* 7.25‰) (Holser 1997; Retallack 1999; Jin *et al.* 2000). Retallack (1999) considered that the plant extinctions and abundant fungal remains recorded in the P/Tr boundary beds in the Sydney Basin, Australia suggest a widespread deforestation. In the Sydney Basin the P/Tr paleosols indicate anomalous warming climate, which was probably triggered by a CO_2 and CH_4 post-apocalyptic greenhouse effect in the high-latitude regions (Retallack 1999). Abundant fungal spores

immediately after plant extinction have also been found in association with a significantly negative shift of $d^{13}C$ excursion in Spitsbergen (Wignall *et al.* 1998; Twitchett *et al.* 2001). Extinction of land vertebrates also coincides with a negative shift of $d^{13}C$ excursion (Ward *et al.* 2005).

Sources of light carbon

As discussed above, a 3% negative shift in $d^{13}C_{carb}$ occurred globally in association with the end-Permian mass extinction, but its cause remains controversial. Here, we consider that this pronounced negative shift in $d^{13}C_{carb}$ could be caused by release of light carbon due to (i) input of mantle carbon ($d^{13}C$ VPDB: 7.5%), (ii) a decrease in biomass ($d^{13}C$ VPDB: 7.27%), (iii) decomposition of sedimentary marine organic matter ($d^{13}C$ VPDB: 7.25%), (iv) denudation of terrestrial organic matter ($d^{13}C$ VPDB: 7.27%), (v) dissociation of methane hydrates ($d^{13}C$ VPDB: 7.60%) deposited in marine sediments, and (vi) an impact of a comet ($d^{13}C$ VPDB: 7.45%) on the Earth. These possible sources are discussed as below.

METHANE HYDRATE

The widespread anoxic deep waters in the latest Permian oceans (Wignall & Twitchett 1996, 2002; Isozaki 1997) suggest the existence of a huge amount of methane hydrate in oceans. Release of CO_2 may have triggered global warming (Kidder & Worsley 2004), which in turn warmed the deep waters resulting in massive dissociation of marine methane hydrate (Dickens *et al.* 1995, 1997; Kaiho *et al.* 1996; Morante 1996; Heydari *et al.* 2000; Liang 2002; Heydari & Hassanzadeh 2003; Riskin 2003; Kump *et al.* 2005; Berner 2006; Riccardi *et al.* 2007). Furthermore, the decomposition of methane hydrate probably accelerated further global warming by an enhanced greenhouse effect of methane gas (and CO_2 , its oxidation product). This scenario of positive feedback for CO_2 release and temperature is consistent with the gradual decrease in $d^{13}C$ and an increase in CO_2 release within * 30 ka before, during and after the end-Permian extinction event (GVZ 2–5).

The high partial pressure of atmospheric CO_2 and climatic warming would have facilitated weathering consuming CO_2 . The elevated CO_2 content in atmosphere would also have caused an increase in dissolved CO_2 in oceans. The weathering and elevated dissolved CO_2 would have resulted in (i) a decrease in atmospheric CO_2 , (ii) cooling and (iii) a halt to the decomposition of methane hydrate, reflected by the recovery of $d^{13}C$ in the lower part of Bed 27.

MIXING OF ANOXIC OCEAN

At Meishan a 1% positive shift at 7.13 to 7.7 cm below the top of Bed 24e (GVZ 1) was observed in both $d^{13}C_{carb}$ and $d^{13}C_{org}$, suggesting oceanic anoxia, which is also indicated by a coincident positive shift of $d^{34}S$ of carbonate-associated sulfate from the same horizon of the same section (Kaiho *et al.* 2001, 2002, 2006a; Riccardi *et al.* 2006, 2007). A decrease in $d^{34}S_{sulfate}$ in Layers 24e-2 and 24e-3 (Kaiho *et al.* 2001) indicates mixing of an

anoxic ocean dominated by H_2S (euxinic ocean: Knoll *et al.* 1996; Hotinski *et al.* 2001; Kaiho *et al.* 2002, 2006a, 2006b; Newton *et al.* 2004; Kump *et al.* 2005; Berner 2006; Riccardi *et al.* 2006, 2007; Gorjan *et al.* 2007, 2008), which suggests oxygenation of organic matter in anoxic, deep-water habitats. Both high TOC (1–2%) and high marine kerogen % (95%) of black fragments in Layer 24e-3 indicate high marine productivity, which suggests a euxinic zone due to ocean mixing (GVZ 3). The 1% negative shift during the mass extinction may have resulted from mixing of anoxic ocean.

INPUT OF MANTLE CARBON

Low values of Sr isotope ratio ($^{87}Sr/^{86}Sr$) of clastics in Layers 24e-2 and 24e-3 indicate input of mantle carbon to the ocean as clastics during and just before the mass extinction (GVZ 3). The Siberian flood basalt volcanism may have provided the source of light carbon because of (i) the coincidence with the end-Permian mass extinction (Renne *et al.* 1995; Kamo *et al.* 2003) and (ii) the huge volume of basalt (Reichow *et al.* 2002). A total of $2-4 \times 10^6$ km³ of volcanic material was released during * 600 ka by the Siberian flood basalt volcanism (Kamo *et al.* 2003). These volcanic activity produced $4-8 \times 10^4$ Gt of CO_2 based on estimates from the comparable Kilauea volcano (Renne *et al.* 1995; Kamo *et al.* 2003). The release of 2.2×10^4 Gt of volcanic CO_2 would generate a 1% negative shift (Kump & Arthur 1999). If all the volcanic material was released within 30 ka, the Siberian flood basalt volcanism could have generated a 2–3% negative shift. However, this is not the case because the release of volcanic material by the Siberian flood basalt volcanism has lasted * 600 ka (Kamo *et al.* 2003).

IMPACT OF A COMET

The presumed impact of a comet at the end of the Permian (Kaiho *et al.* 2001) may have caused the release of an enormous amount of carbon. A normal-sized (* 10 km diameter) comet and a maximum-sized (20 km diameter) comet can release 2×10^2 Gt and 2×10^3 Gt carbon, respectively, based on Greenberg's (1998) estimation that a comet's organic carbon ($d^{13}C$: 7.45%) content is 20%. The release of CO_2 from a comet, 10–20 km in diameter, could cause a 0.2–1.6% decrease in $d^{13}C$ within the entire ocean-atmosphere system in less than 1 ka, based on 4×10^4 Gt of carbon in the ocean. However, a cometary impact should result in a rapid $d^{13}C$ decrease in the atmosphere and oceanic surface waters. As such, a cometary impact cannot explain the gradual decrease in $d^{13}C$ obtained from the mid-Bed 24e-1 to Bed 26, although an impact of a comet may be responsible for small negative shifts (0.2%) in both $d^{13}C_{carb}$ and $d^{13}C_{org}$ values recorded between Bed 25-1 and basal Bed 26 (GVZ 4).

DENUATION OF TERRESTRIAL MATTER

The coincidence of maxima in TOC percentage and Sr isotope ratio of clastics in Bed 26 (Figure 2) indicates

that significant denudation of terrestrial sediments occurred within * 27 ka after the main extinction (GVZ 5). The mass extinction of terrestrial plants and devastation of forests (Retallack 1995, 1999; Sephton *et al.* 2005) caused massive erosion of soil and sediment and a significant release of CO₂—the latter generating isotopically light carbon (* 7.28%). Devastation of plants also results in a decrease in absorption of CO₂ and an increase in isotopically light carbon in the atmosphere, which facilitates an increase in CO₂ and a decrease in d¹³C in the atmosphere. The denudation of terrestrial organic matter could be responsible for the negative shifting of d¹³C recorded in Bed 26 (GVZ 5). This view is strengthened by recent molecular geochemical analysis from the same section (Wang 2007; Wang & Visscher 2007).

CONCLUSIONS

A 3‰ negative shift of d¹³C_{carb} values occurred globally at the end of the Permian. In Meishan carbon isotopic excursions (d¹³C_{carb}, d¹³C_{org}) coupled with other geochemical signals show six geochemical variation zones (GVZ) over the end-Permian extinction, with GVZ 1 corresponding to the lower-middle parts of Bed 24e-1, GVZ 2 to the upper Bed 24e-1, GVZ 3 to Beds 24e-2, 24e-3, 25-1 and 25-2, GVZ 4 to Bed 25-3, GVZ 5 to Bed 26 and GVZ 6 to Beds 27–29. A coincidental 3‰ negative shift observed in d¹³C of marine bulk carbonate (supported by d¹³C of brachiopod shell) and all organic matter just before, during and after the end-Permian mass extinction confirms that the significant light carbon release occurred * 13 ka before, * 5 ka during and * 13 ka after the extinction event. A 7.1‰ shift of d¹³C excursion before the extinction was probably generated by possible dissociation of methane hydrate by warming (GVZ 2). Both mixing of anoxic ocean and dissociation of methane hydrate led to another 7.1‰ shift of d¹³C during the end-Permian extinction (GVZ 3). The further 7.1‰ shift of d¹³C after the extinction has probably resulted from massive denudation of soil and sediment caused by the collapse of continental ecosystems as well as possible dissociation of methane hydrate at the end of the Permian (GVZ 5). A dramatic decrease in D¹³C across the main extinction horizon indicates that phototrophic sulfur bacteria abruptly proliferated immediately after the end-Permian event. Low D¹³C values throughout Beds 27–29 imply that phototrophic sulfur bacteria may have thrived more than 150 ka after the main extinction. An abrupt increase in D¹³C in Bed 26 further confirms that massive denudation of soil and sediment caused by the collapse of continental ecosystems after the end-Permian mass extinction.

ACKNOWLEDGEMENTS

We are thankful to G. R. Dickens and J. C. Ingle for comments on an earlier draft. The critical reviews by two journal reviewers have improved the quality of the paper. This work was partly supported by a grant-in-aid

for scientific research from the Ministry of Education, Science and Culture of Japan (to KK and ZQC) and a discovery grant (DP 0770938) from the Australia Research Council (to ZQC). This study is a contribution to the IGCP 572 'Permian–Triassic ecosystems'.

REFERENCES

- BAUD A., MAGARITZ M. & HOLSER W. T. 1989. Permian–Triassic of the Tethys: carbon isotope studies. *Geologische Rundschau* **78**, 649–677.
- BERNER R. A. 2002. Examination of hypotheses for the Permo–Triassic boundary extinction by carbon cycle modelling. *Proceedings of the National Academy of Sciences* **99**, 4172–4177.
- BERNER R. A. 2006. Carbon, sulphur and O₂ across the Permian–Triassic boundary. *Journal of Geochemical Exploration* **88**, 416–418.
- BOUSSAFIR M., GELIN F., LALLIER-VERGES E., DERENNE S., BERTRAND P. & LARGEAU C. 1995. Electron microscopy and pyrolysis of kerogens from the Kimmeridge Clay Formation, UK: source organisms, preservation processes, and origin of microcycles. *Geochimica et Cosmochimica Acta* **59**, 3731–3747.
- BOWRING S. A., ERWIN D. H., JIN Y. G., MARTIN M. W., DAVID E. K. & WANG W. 1998. U/Pb zircon geochronology and tempo of the end-Permian mass extinction. *Science* **280**, 1039–1045.
- BOWRING S. A., RAMEZANI J., CROWLEY J. & CONDON D. 2007. Earthtime: a community-based initiative for calibrating geological time. In: Wang Y., Zhang H. & Wang X. eds. *Abstracts of the 16th International Congress on the Carboniferous and Permian*, p. 2. *Journal of Stratigraphy* **31** (Supplement 1).
- CAO C., WANG W. & JIN Y. 2002. Carbon isotope excursions across the Permian–Triassic boundary in the Meishan section, Zhejiang Province, China. *Chinese Science Bulletin* **47**, 1125–1129.
- CHAI C., ZHOU Y., MAO X., MA S., MA J., KONG P. & HE J. 1992. Geochemical constraints on the Permo–Triassic boundary event in South China. In: Sweet W. C., Yang Z., Dickins J. M. & Yin H. eds. *Permo–Triassic events in the Eastern Tethys: stratigraphy, classification, and relations with the Western Tethys*, pp. 158–168. Cambridge University Press, Cambridge.
- CHEN Z. Q., KAIHO K. & GEORGE A. D. 2005. Survival strategy of brachiopod fauna from the end-Permian mass extinction. *Palaeogeography, Palaeoclimatology, Palaeoecology* **224**, 232–269.
- CHEN Z. Q., SHI G. R. & KAIHO K. 2002. A new genus of rhynchonellid brachiopod from the Lower Triassic of South China and implications for timing the recovery of Brachiopoda after the end-Permian mass extinction. *Palaeontology* **45**, 149–164.
- CORSETTI F. A., BAUD A., MARENCO P. J. & RICOZ S. 2005. Summary of Early Triassic carbon isotope records. *Comptes Rendus Palevol* **4**, 473–486.
- DICKENS G. R., O'NEIL J. R., REA D. K. & OWEN R. M. 1995. Dissociation of oceanic methane hydrate as a cause of the carbon isotope excursion at the end of the Paleocene. *Paleoceanography* **10**, 965–971.
- DICKENS G. R., CASTILLO M. M. & WALKER J. C. G. 1997. A blast of gas in the latest Paleocene: simulating first-order effects of massive dissociation of oceanic methane hydrate. *Geology* **25**, 258–262.
- DOLENEC T., LOJEN S. & RAMOVŠ A. 2001. The Permian–Triassic boundary in Western Slovenia (Idrija Valley section): magnetostratigraphy, stable isotopes, and elemental variations. *Chemical Geology* **175**, 175–190.
- ERWIN D. H. 1993. *The Great Paleozoic Crisis*. Columbia University Press, New York.
- ERWIN D. H. 1994. The Permo–Triassic extinction. *Nature* **367**, 231–236.
- ERWIN D. H., BOWRING S. A. & YUGAN J. 2002. End-Permian mass extinctions: a review. In: Koeberl C. & MacLeod K. G. eds. *Catastrophic events and mass extinctions: impacts and beyond*, pp. 363–383. Geological Society of America Special Paper **356**.
- GHOSH P., BHATTACHARYA S. K., SHUKLA A. D., SHUKLA P. N., BHANDARI N., PARTHASARATHY G. & KUNWAR A. C. 2002. Negative d¹³C excursion and anoxia at the Permo–Triassic boundary in the Tethys Sea. *Current Science* **83**, 498–502.

- GORJAN P., KAIHO K. & CHEN Z. Q. 2008. A carbon-isotopic study of an end-Permian mass-extinction horizon, Bulla, northern Italy: a negative delta C-13 shift prior to the marine extinction. *Terra Nova* **20**, 252–258.
- GORJAN P., KAIHO K., KAKEYAWA T., NIITSUMA S., CHEN Z. Q., KAJIWARA Y. & NICORA A. 2007. Paleoredox, biotic and sulfur-isotopic changes associated with the end-Permian mass extinction in the western Tethys. *Chemical Geology* **244**, 483–492.
- GREENBERG J. M. 1998. Making a comet nucleus. *Astronomy and Astrophysics* **330**, 375–380.
- GRICE K., CAO C., LOVE G. D., BÖTTCHER M. E., TWITCHETT R. J., GROSJEAN E., SUMMONS R. E., TURGEON S. C., DUNNING W. & JIN Y. 2005. Photic zone euxinia during the Permian–Triassic super-anoxic event. *Science* **307**, 706–709.
- HEYDARI E. & HASSANZADEH J. 2003. Deev Jahi Model of the Permian–Triassic boundary mass extinction: a case for gas hydrates as the main cause of biological crisis on Earth. *Sedimentary Geology* **163**, 147–163.
- HEYDARI E., HASSANZADEH J. & WADE W. J. 2000. Geochemistry of central Tethyan Upper Permian and Lower Triassic strata, Abadeh region, Iran. *Sedimentary Geology* **137**, 85–99.
- HEYDARI E., WADE W. J. & HASSANZADEH J. 2001. Diagenetic origin of carbon and oxygen isotope compositions of Permian–Triassic boundary strata. *Sedimentary Geology* **143**, 191–197.
- HOLSER W. T. 1997. Geochemical events documented in inorganic carbon isotopes. *Palaeogeography Palaeoclimatology Palaeoecology* **132**, 173–182.
- HOLSER W. T., SCHOENLAUB H. P., ATTREP M. JR, BOECKELMANN K., KLEIN P., MAGARITZ M., ORTH C. J., FENNINGER A., JENNY C., KRALIK M., MAURITSCH H., PAK E., SCHRAMM J. M., STATTEGGER K. & SCHMOELLER R. 1989. A unique geochemical record at the Permian–Triassic boundary. *Nature* **337**, 39–44.
- HOTINSKI R. M., BICE K. L., KUMP L. R., NAJIAR R. G. & ARTHUR M. A. 2001. Ocean stagnation and end-Permian anoxia. *Geology* **29**, 7–10.
- ISOZAKI Y. 1997. Permo-Triassic boundary superanoxia and stratified superocean: records from lost deep sea. *Science* **276**, 235–238.
- JIN Y. G., WANG Y., WANG W., SHANG Q. H., CAO C. Q. & ERWIN D. H. 2000. Pattern of marine mass extinction near the Permian–Triassic boundary in south China. *Science* **289**, 432–436.
- KAIHO K., ARINOBU T., ISHIWATARI R., MORGANS H. E. G., OKADA H., TAKEDA N., TAZAKI K., ZHOU G., KAJIWARA Y., MATSUMOTO R., HIRAI A., NIITSUMA N. & WADA H. 1996. Latest Paleocene benthic foraminiferal extinction and environmental changes at Tawanui, New Zealand. *Paleoceanography* **11**, 447–465.
- KAIHO K., CHEN Z. Q., MIURA Y., KAWAHATA H., KAJIWARA Y. & SATO H. 2006a. Close-up of the end-Permian mass extinction horizon recorded in the Meishan section, South China: sedimentary, elemental, and biotic characterization with a negative shift of sulfate sulfur isotope ratio. *Palaeogeography, Palaeoclimatology, Palaeoecology* **239**, 396–405.
- KAIHO K., KAJIWARA Y., CHEN Z. Q. & GORJAN P. 2006b. A sulfur isotope event at the end of the Permian. *Chemical Geology* **235**, 33–47.
- KAIHO K., KAJIWARA Y. & MIURA Y. 2002. End-Permian catastrophe by a bolide impact: evidence of a gigantic release of sulfur from the mantle: Comment and Reply: Reply. *Geology* **30**, 856.
- KAIHO K., KAJIWARA Y., NAKANO T., MIURA Y., KAWAHATA H., TAZAKI K., UESHIMA M., CHEN Z. Q. & SHI G. R. 2001. End-Permian catastrophe by a bolide impact: evidence of a gigantic release of sulfur from the mantle. *Geology* **29**, 815–818.
- KAMO S. L., CZAMANSKE G. K. & AMELIN Y., FEDORENKO V. A., DAVIS D. W. & TROFIMOV V. R. 2003. Rapid eruption of Siberian flood-volcanic rocks and evidence for coincidence with the Permian–Triassic boundary and mass extinction at 251 Ma. *Earth and Planetary Science Letters* **214**, 75–91.
- KIDDER D. L. & WORSLEY T. R. 2004. Causes and consequences of extreme Permo-Triassic warming to globally equable climate and relation to the Permo-Triassic extinction and recovery. *Palaeogeography, Palaeoclimatology, Palaeoecology* **203**, 207–237.
- KNOLL A. K., BAMBACH R. K., CANFIELD D. E. & GROTSINGER J. P. 1996. Comparative earth history and Late Permian mass extinction. *Science* **273**, 452–457.
- KRULL E. S., LEHRMANN D. J., DRUKE D., KESSEL B., YU Y. Y. & LI R. 2004. Stable carbon isotope stratigraphy across the Permian–Triassic boundary in shallow marine carbonate platforms, Nanpanjiang Basin, south China. *Palaeogeography, Palaeoclimatology, Palaeoecology* **204**, 297–315.
- KRULL E. S. & RETALLACK G. L. 2000. $\delta^{13}\text{C}$ depth profile from paleosols across the Permian–Triassic boundary: evidence for methane release. *Geological Society of America Bulletin* **112**, 1459–1472.
- KRULL E. S., RETALLACK G. L., CAMPBELL H. J. & LYON G. L. 2000. $\delta^{13}\text{C}_{\text{org}}$ chemostratigraphy of the Permian–Triassic boundary in the Maitai Group, New Zealand: evidence for high-latitude methane release. *New Zealand Journal of Geology and Geophysics* **43**, 21–32.
- KUMP L. R. & ARTHUR M. A. 1999. Interpreting carbon-isotope excursions: carbonates and organic matter. *Chemical Geology* **161**, 181–198.
- KUMP L. R., PAVLOV A. & ARTHUR M. A. 2005. Massive release of hydrogen sulfide to the surface ocean and atmosphere during intervals of oceanic anoxia. *Geology* **33**, 397–400.
- LAMARQUE J. F., KIEHL J. T. & ORLANDO J. J. 2007. Role of hydrogen sulphide in a Permian–Triassic boundary ozone collapse. *Geophysical Research Letters* **34**, L02801 (1–4), doi:10.1029/2006GL028384, 2007.
- LI Z., ZHANG J., JUN R., LIU G., SHENG H., SHEN G., DAI J., HUANG H., XIE L., YAN Z. & YAO J. 1986. Mass extinction and geological events between Palaeozoic and Mesozoic era. *Acta Geologica Sinica* **60**, 1–15.
- LIANG H. 2002. End-Permian catastrophic event of marine acidification by hydrated sulfuric acid: mineralogical evidence from Meishan section of South China. *Chinese Science Bulletin* **47**, 1393–1397.
- MAGARITZ M., BAR R., BAUD A. & HOLSER W. T. 1988. The carbon isotope shift at the Permian/Triassic boundary in the southern Alps is gradual. *Nature* **331**, 337–339.
- MORANTE R. 1996. Permian and Early Triassic isotopic records of carbon and strontium in Australia and a scenario of events about the Permian–Triassic boundary. *Historical Biology* **11**, 289–310.
- MORANTE R., VEEVERS J. J., ANDREW A. S. & HAMILTON P. J. 1994. Determining the Permian/Triassic boundary in Australia using C-isotope chemostratigraphy. *APEA Journal* **34**, 330–336.
- MUNDIL R., LUDWIG K. R., METCALFE I. & RENNE P. R. 2004. Age and timing of the Permian mass extinctions: U/Pb dating of closed-system zircons. *Science* **305**, 1760–1763.
- MUNDIL R., METCALFE I., LUDWIG K. R., RENNE P. R., OBERLI F. & NICOLL R. S. 2001. Timing of the Permian–Triassic biotic crisis: implications from new zircon U/Pb age data (and their limitations). *Earth and Planetary Science Letters* **187**, 131–145.
- MUSASHI M., ISOZAKI Y., KOIKE T. & KREULEN R. 2001. Stable carbon isotope signature in mid-Panthalassa shallow-water carbonates across the Permo-Triassic boundary: evidence for ^{13}C -depleted superocean. *Earth and Planetary Science Letters* **191**, 9–20.
- NEWTON R. J., PEVITT E. L., WIGNALL P. B. & BOTTRELL S. H. 2004. Large shifts in the isotopic composition of seawater sulphate across the Permo-Triassic boundary in northern Italy. *Earth and Planetary Science Letters* **218**, 331–345.
- OBOH-IKUENOBE F. E., YEPES O. & ODP LEG 159 SCIENTIFIC PARTY, 1997. Palynofacies analysis of sedimentary from the Côte d'Ivoire–Ghana transform margin: preliminary correlation with some regional events in the Equatorial Atlantic. *Palaeogeography, Palaeoclimatology, Palaeoecology* **29**, 291–314.
- PAYNE J. L., LEHRMANN D. J., WEI J., ORCHARD M. J., SCHRAG D. P. & KNOLL A. H. 2004. Large perturbations of the carbon cycle during recovery from the end-Permian extinction. *Science* **305**, 506–509.
- PENG Y., ZHANG S., YU T., YANG F., GAO Y. & SHI G. R. 2005. High-resolution terrestrial Permian–Triassic eventostratigraphic boundary in western Guizhou and eastern Yunnan, southwestern China. *Palaeogeography, Palaeoclimatology, Palaeoecology* **215**, 285–295.
- REICHOW M. K., SAUNDERS A. D., WHITE R. V., PRINGLE M. S., AL'MUKHAMEDOV A. I., MEDVEDEV A. I. & KIRDA N. P. 2002. $^{40}\text{Ar}/^{39}\text{Ar}$ dates from the West Siberian Basin: Siberian flood basalt province doubled. *Science* **296**, 1846–1849.
- RENNE P. R., ZHANG Z. C., RICHARDS M. A., BLACK M. T. & BASU A. R. 1995. Synchrony and causal relations between Permian–Triassic boundary crisis and Siberian flood volcanism. *Science* **269**, 1413–1416.
- RETALLACK G. J. 1995. Permian–Triassic extinction on land. *Science* **267**, 77–80.
- RETALLACK G. J. 1999. Postapocalyptic greenhouse paleoclimate revealed by earliest Triassic paleosols in the Sydney Basin, Australia. *Geological Society of America Bulletin* **111**, 52–70.

- RESTALLACK G. J., SEYEDOLALI A., KRULL E. S., HOLSER W. T., AMBERS, C. P. & KYTE F. T. 1998. Search for evidence of impact at the Permian-Triassic boundary in Antarctica and Australia. *Geology* **26**, 979–982.
- RICCARDI A. L., ARTHUR M. A. & KUMP L. R. 2006. Sulfur isotopic evidence for chemocline upward excursions during the end-Permian mass extinction. *Geochimica et Cosmochimica Acta* **70**, 5740–5752.
- RICCARDI A. L., KUMP L. R., ARTHUR M. A. & D'HONDT S. 2007. Carbon isotopic evidence for chemocline upward excursions during the end-Permian event. *Palaeogeography, Palaeoclimatology, Palaeoecology* **248**, 73–81.
- RISKIN G. 2003. Methane-driven oceanic eruptions and mass extinctions. *Geology* **31**, 741–744.
- SARKAR A., YOSHIOKA H., EBIHARA M. & NARAOKA H. 2003. Geochemical and organic carbon isotope studies across the continental Permo-Triassic boundary of Raniganj basin, Eastern India. *Palaeogeography, Palaeoclimatology, Palaeoecology* **191**, 1–14.
- SAWADA K. & AKIYAMA M. 1994. Carbon isotope composition of macerals separated from various kerogens by density separation method. *Journal of the Japanese Association for Petroleum Technology* **59**, 244–255.
- SEPTON M. A., LOOY C. V., BRINKHUIS H., WIGNALL P. B., LEEUW J. W. DE & VISSCHER H. 2005. Catastrophic soil erosion during the end-Permian biotic crisis. *Geology* **33**, 941–944.
- SHENG J., CHEN C., WANG Y., RUI L., LIAO Z., BANDO Y., ISHII K., NAKAZAWA K. & NAKAMURA K. 1984. Permian-Triassic boundary in middle and Eastern Tethys. *Journal of Faculty of Science Hokkaido University Series 4* **21**, 133–181.
- SMITH P. M. R. 1984. The use of fluorescence microscopy in the characterization of amorphous organic matter. *Organic Geochemistry* **6**, 839–845.
- TWITCHETT R. J., LOOY C. V., MORANTE R., VISSCHER H. & WIGNALL P. B. 2001. Rapid and synchronous collapse of marine and terrestrial ecosystems during the end-Permian mass extinction event. *Geology* **29**, 351–354.
- VAN BREUGEL Y., SCHOUTEN S., PAETZEL M., OSSEBAAR J. & SINNINGHE DAMSTE J. S. 2005. Reconstruction of $\delta^{13}\text{C}$ of chemocline CO_2 (aq) in past oceans and lakes using the $\delta^{13}\text{C}$ of fossil isorenieratene. *Earth and Planetary Science Letters* **235**, 421–434.
- WANG C. 2007. Anomalous hopane distributions at the Permian-Triassic boundary, Meishan, China—evidence of the end-Permian marine ecosystem collapse. *Organic Geochemistry* **38**, 52–66.
- WANG C. & VISSCHER H. 2007. Abundance anomalies of aromatic biomarkers in the Permian-Triassic boundary section at Meishan, China—evidence of end-Permian terrestrial ecosystem collapse. *Palaeogeography, Palaeoclimatology, Palaeoecology* **252**, 291–303.
- WANG K., GELDSETZER H. H. J. & KROUSE H. R. 1994. Permian-Triassic extinction: organic $\delta^{13}\text{C}$ evidence from British Columbia, Canada. *Geology* **22**, 580–584.
- WARD P. D., BOTHA J., BUICK R., DE KOCK M. O., ERWIN D. H., GARRISON G. H., KIRSCHVINK J. L. & SMITH R. 2005. Abrupt and gradual extinction among Late Permian land vertebrates in the Karoo Basin, South Africa. *Science* **307**, 709–714.
- WIGNALL P. B., MORANTE R. & NEWTON R. 1998. The Permo-Triassic transition in Spitsbergen: $\delta^{13}\text{C}_{\text{org}}$ chemostratigraphy, Fe and S geochemistry, facies, fauna and trace fossils. *Geological Magazine* **135**, 47–62.
- WIGNALL P. B. & TWITCHETT R. J. 1996. Oceanic anoxia and the end-Permian mass extinction. *Science* **272**, 1155–1158.
- WIGNALL P. B. & TWITCHETT R. J. 2002. Extent, duration and nature of the Permian-Triassic superanoxic event. In: Koeberl C. & MacLeod K. G. eds. *Catastrophic events and mass extinctions: impacts and beyond*, pp. 395–413. Geological Society of America Special Paper **356**.
- WIT M. J., DE GHOSCH J. G., VILLIERS S. DE, RAKOTOSOLOFO N., ALEXANDER J., TRIPATHI A. & LOOY C. 2002. Multiple organic carbon isotope reversals across the Permo-Triassic Boundary of terrestrial Gondwana sequences: clues to extinction patterns and delayed ecosystem recovery. *Journal of Geology* **110**, 227–240.
- XIE S., PANCOST R. D., HUANG X., JIAO D., LU L., HUANG J., YANG F. & EVERSHERD R. P. 2007a. Molecular and isotopic evidence for episodic environmental change across the Permo/Triassic boundary at Meishan in South China. *Global and Planetary Change* **55**, 56–65.
- XIE S., PANCOST R. D., HUANG J., WIGNALL P. B., YU J., TANG X., CHEN L., HUANG X. & LAI X. 2007b. Changes in the global carbon cycle occurred as two episodes during the Permian-Triassic crisis. *Geology* **35**, 1083–1086.
- XIE S., PANCOST R. D., YIN H., WANG H. & EVERSHERD R. P. 2005. Two episodes of microbial change coupled with Permo/Triassic faunal mass extinction. *Nature* **434**, 494–497.
- XU D. Y. & YAN Z. 1993. Carbon isotope and iridium event markers near the Permian/Triassic boundary in the Meishan section, Zhejiang Province, China. *Palaeogeography, Palaeoclimatology, Palaeoecology* **104**, 171–176.
- XU D. Y., ZHANG Q. W., SUN Y. Y., YAN Z., HAI Z. F. & HE J. W. 1989. *Astrogeological events in China*. Scottish Academic Press, Edinburgh.
- YIN H., FENG Q., BAUD A., XIE S., BENTON M. J., LAI X. & BOTTJER D. J. 2007a. The prelude of the end-Permian mass extinction predates a postulated bolide impact. *International Journal of Earth Science* **96**, 903–909.
- YIN H., FENG Q., LAI X., BAUD A. & TONG J. 2007b. The protracted Permo-Triassic crisis and multi-episode extinction around the Permian-Triassic boundary. *Global and Planetary Changes* **55**, 1–20.
- YIN H., HUANG S., ZHANG K., HANSEN H. J., YANG F., DING M. & BIE X. 1992. The effects of volcanism on the Permo-Triassic mass extinction in South China. In: Sweet W. C., Yang Z., Dickins J. M. & Yin H. eds. *Permo-Triassic events in the Eastern Tethys: stratigraphy, classification, and relations with the Western Tethys*, pp. 146–157. Cambridge University Press, Cambridge.
- YIN H., ZHANG K., TONG J., YANG Z. & WU S. 2001. The Global Stratotype Section and Point (GSSP) of the Permian-Triassic boundary. *Episodes* **24**, 102–114.
- ZHANG K., TONG J., YIN H. & WU S. 1996. Sequence stratigraphy near the Permian-Triassic boundary at Meishan section, South China. In: Yin H. ed. *The Palaeozoic-Mesozoic Boundary candidates of Global Stratotype Section and Point of the Permian-Triassic Boundary*, pp. 72–83. China University of Geosciences Press, Wuhan, China.
- ZIEGLER A. M., GIBBS M. T. & HULVER M. L. 1998. A mini-atlas of oceanic water masses in the Permian Period. *Proceedings of the Royal Society of Victoria* **110**, 323–343.

Received 10 September 2007; accepted 4 April 2009